JOURNAL OF SPACECRAFT AND ROCKETS
Vol. 31, No. 5, September–October 1994

Structural and Loads Analysis of a Two-Stage Reusable Manned Launch System

James C. Robinson*
Old Dominion University Research Foundation, Hampton, Virginia 23681
and
Douglas O. Stanley†
NASA Langley Research Center, Hampton, Virginia 23681

The conceptual design of a rocket-powered, two-stage, fully reusable launch vehicle has been performed as a part of the NASA's Advanced Manned Launch System study. This paper summarizes the structural design and load analysis of this vehicle. The method used to determine the structural weights consists of generating a finite-element model for each vehicle, selecting a set of critical loading conditions, determining the loads on the model caused by those conditions, determining the model response, and changing the sizes of individual elements to obtain a safe structure. The integrated loads on the vehicle were obtained from a three-degree-of-freedom trajectory analysis.

Nomenclature

g	= acceleration of gravity at Earth's surface, 32.2 ft/s^2
q	= dynamic pressure, lb/ft^2
T/W	= thrust-to-weight ratio
α	= angle of attack, degrees
ΔV	= incremental velocity, ft/s

Introduction

IN recent years, NASA has begun studies to define options for the next manned space transportation system. The goals of this broad NASA effort are to define systems that meet future mission requirements of transporting personnel and payloads requiring a manned presence, while emphasizing improved cost-effectiveness, increased vehicle reliability and personnel safety, and large operational margins. Three approaches are being examined for satisfying future manned-launch needs. One approach is the evolution of the current Space Shuttle. Another is the definition of a small Personnel Launch System (PLS) for carrying people and small amounts of cargo to and from space. The third approach is that of a new, more operationally efficient Advanced Manned Launch System (AMLS) to replace the present Space Shuttle.[1]

The goals of the AMLS study are to examine systems that provide routine, lower-cost manned access to space. Technologies and system approaches are being studied that will contribute to significant reductions in operating costs relative to current systems. A wide variety of vehicle types and propulsion systems has been examined in the conceptual and preliminary design of next-generation manned-launch systems as a part of the AMLS study. These include single-stage and two-stage systems, systems utilizing rocket and air-breathing propulsion, and systems with varying degrees of reusability.[2] For the assumed flight rate, payload class, and technology readiness, a rocket-powered, two-stage, fully reusable system was selected for detailed study. This vehicle would be expected to have a 2005–2010 initial operating capability in order to gradually replace an aging Shuttle fleet. Hence, a 1995–2000 technology readiness date has been assumed to represent normal-growth (evolutionary) technology advancements in vehicle structure, propulsion, and subsystems. Although many of these assumed technological advancements contribute to significant weight savings in the vehicle, a portion of these saving has been applied to aspects of vehicle design that enhance the operations, reliability, and safety factors of the system.[1]

This paper summarizes the structural design and loads analysis of this launch vehicle. The method used to determine the structural weights consists of generating a finite-element model for each vehicle, selecting a set of critical loading conditions, determining the loads on the model caused by those conditions, determining the model response and changing the sizes of individual elements to obtain a safe structure. The integrated loads on the vehicle were obtained from an optimal three-degree-of-freedom (3-DOF) trajectory analysis.

Analysis Methodology

The integrated structural design of next-generation rocket-powered launch systems requires proper consideration of the effects of the vehicle geometry, trajectory, and aerodynamics. All of the geometry and subsystem packaging is performed using the NASA-developed Solid Modeling Aerospace Research Tool (SMART) geometry package. SMART is a menu-driven interactive computer program for generating three-dimensional Bézier-surface representations of aerospace vehicles for use in aerodynamic and structural analysis.[3] All of the trajectory analysis is performed using the 3-DOF version of Program to Optimize Simulated Trajectories (POST). POST is a generalized point-mass, discrete-parameter targeting and optimization program that allows the user to target and optimize point-mass trajectories for a powered or unpowered vehicle near an arbitrary rotating, oblate planet.[4] The Aerodynamic Preliminary Analysis System (APAS) is used to determine vehicle aerodynamics. In the subsonic and low supersonic speed regimes, APAS utilizes slender-body theory, viscous- and wave-drag empirical techniques, and source and vortex panel distributions to estimate the vehicle aerodynamics. At high supersonic and hypersonic speeds, a noninterference finite-element model of the vehicle is analyzed using empirical impact-pressure methods and approximate skin-friction methods.[5]

The method used for structural analysis and weight determination includes geometry modeling, finite-element modeling, load generation and application, finite-element analysis, element sizing to meet loading conditions and structural criteria, and structural-element weight summation, organized into an iterative process. This process is illustrated in Fig. 1. The external shape of a vehicle configuration can be modeled by discretizing a SMART geometry into a finite-

Presented as Paper 92-4774 at the AIAA/USAF/NASA/OAI Fourth Symposium on Multidisciplinary Analysis and Optimizations, Cleveland, OH, Sept. 21–23, 1992; received Feb. 6, 1993; accepted for publication by Jan. 4, 1994.

*Aerospace Engineer; mailing address: NASA Langley Research Center, MS 365. Member AIAA.

†Aerospace Engineer, Space Systems Division. Member AIAA.

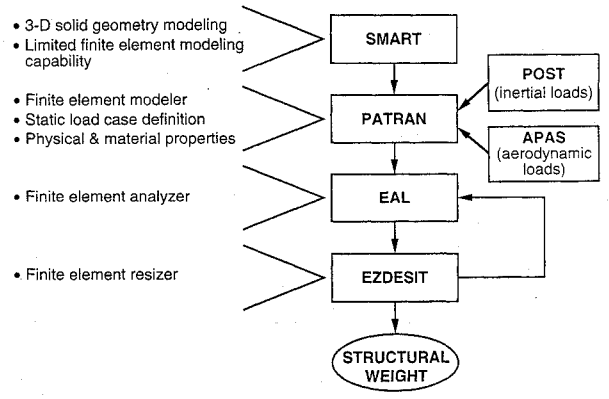

Fig. 1 Structural-analysis methodology.

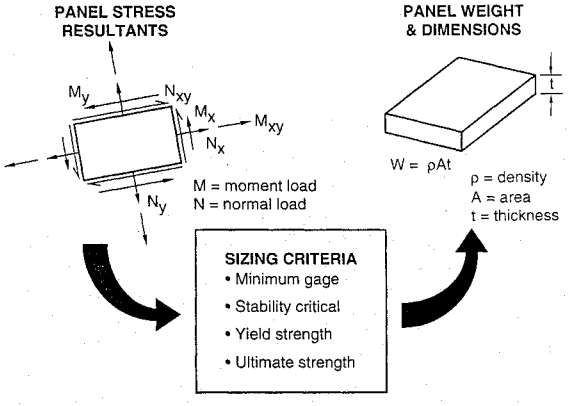

Fig. 2 Panel sizing methodology.

element model (FEM) through the use of PATRAN.[6] For relatively simple geometries, a FEM can be constructed directly. Experience is then used to initially determine and model the internal structure of the vehicle. Physical and material properties of the structure are included in the FEM of the vehicle. Mission static-load cases are assembled from critical POST inertial loads and APAS aerodynamic loads. The completed finite-element structural model with physical and material properties, external loading, and structural arrangement is then ready for analysis.

Engineering Analysis Language[7] (EAL) is used for the finite-element analysis. The analysis produces resultant structural loads due to the loading conditions for each element. The responses determined by EAL for the loading conditions include displacements and reactions, stresses, buckling loads, and strain-energy densities. The resultant loads are indicative of the load paths of the vehicle structure. These loads are applied to the EZDESIT program[8] to size the finite elements (bars, planar beams, and plate elements) to withstand the loading conditions as shown in Fig. 2. The cross-sectional areas of bar elements are sized. The cap cross-sectional areas and web height and thickness are sized for planar beams. The plate element design variables depend on the type of construction chosen. Isotropic and composite honeycomb, hat-stiffened, and membrane panels along with corrugated web elements can be sized by the code. For each element, a stiffness matrix and a construction geometry (lamina gauge, honeycomb core height, etc.) are specified, and each element has an initial thickness equal to the minimum gauge value. The elements are sequentially checked for failure due to panel buckling, yield, and ultimate modes for each loading case. If failure occurs, the element dimensions are increased until the indicated failure mode is satisfied. The geometric sizing of the panel alters the stiffness properties. Thus, the finite-element analysis and geometry sizing are iterated until convergence is achieved.

Resizing of structural elements to increase the global buckling strength of the structure is accomplished after completion of the strength sizing. Local buckling constraints are satisfied in the strength sizing in EZDESIT. The method uses EAL-generated element strain-energy densities to calculate scaling factors that are applied to EZDESIT element dimension files. The global-buckling sizing method is described in Appendix A. Scaling factors are calculated using values for the first buckling mode of the loading conditions that caused global buckling in the strength-sized structure below ultimate load. This method provides a satisfactory structure but does not optimize the solution.

The dominant load case for each element is determined, and its corresponding dimensions, weight, and failure mode are obtained. The results of the sizing can be reviewed in two different manners. The resulting weights can be grouped by failure mode, element type, load case, and component, or the EZDESIT output file can be read into PATRAN and the element properties displayed on the model. Those properties include internal loads, dominant load case, failure modes, and unit weights. Highly stressed areas may indicate a need for an alternative structural design. Resultant loads are reviewed by the structural designer, and the necessary changes to the structural arrangement are made by altering the FEM and reanalyzing the structure.

Vehicle Concept

Mission and Guidelines

The design reference mission for the two-stage fully reusable AMLS vehicle calls for the delivery and return of up to 40,000 lb of payload from Kennedy Space Center (KSC) to Space Station Freedom (220 n.mi., 28.5-deg inclination) along with a crew of ten (eight passengers and a two-person flight crew). A three-day flight duration with an in-flight margin was budgeted (35 man-days). The payload bay dimensional requirements were 15-ft diam by 30-ft length. On-board propellant world provide an incremental velocity (ΔV) of 1350 ft/s following launch insertion into a 50 × 100-n.mi. orbit. Landing would nominally be at the KSC launch site.

The AMLS vehicle was designed with a crew escape capability characterized by the jettisoning of the crew module using high-impulse solid rocket motors with in-flight stabilization followed by the deployment of a parachute system for landing. In addition, both the booster and the orbiter have single-engine-out capability from liftoff for added reliability and mission success. A 15% dry-weight growth margin was also allocated. The orbiter was required to have a 1100-n.mi. crossrange capability to allow once-around abort for launch to a polar orbit and to increase daily landing opportunities to selected landing sites. All trajectories for this vehicle have maximum acceleration limits of 3 g and normal load constraints on the wings equivalent to a 2.5 g subsonic pullup maneuver.

Vehicle Configuration

The AMLS vehicle, shown in Fig. 3, is a two-stage, parallel-burn design that consists of a manned orbiter and an unmanned winged booster that stages at a Mach number of 3 and glides back to the launch site. Propellants are crossfed from the booster to the orbiter during the boost phase, so that the orbiter's propellant tanks are full at staging. Both the booster and orbiter use liquid hydrogen (LH2) and liquid oxygen (LO2) as propellants. The orbiter also employs a detachable payload canister concept to allow off-line processing of payloads and rapid payload integration. Both booster and orbiter are control-configured and employ wing-tip fins for lateral control. Integral, reusable cryogenic propellant tanks are used on both the booster and orbiter. Dual-lobed tanks are used on the orbiter to allow the external payload canister to be easily integrated and for aerodynamic and re-entry heating considerations. As shown in the figure, the total vehicle dry weight is 343,000 lb, and the gross weight is 2,604,000 lb. The total liftoff thrust-to-weight ratio (T/W) of the vehicle is 1.3. The reference AMLS orbiter utilizes five light-weight derivatives of the Space Shuttle Main Engine for main propulsion, whereas the reference booster uses five of the same engines with a lower-area-ratio nozzle. These engines are throttled to 80% of rated thrust for normal operation to provide single-engine-out capability on each stage and to increase individual engine life. Both the booster and the orbiter utilize an internally stiffened ring-frame construction with carrier panels and durable metallic thermal-protection-system tile sections attached to insulated standoffs where appropriate.

Structural Configuration

The construction of the orbiter and booster of the AMLS utilizes near-term technology. The main propellant tanks are assumed

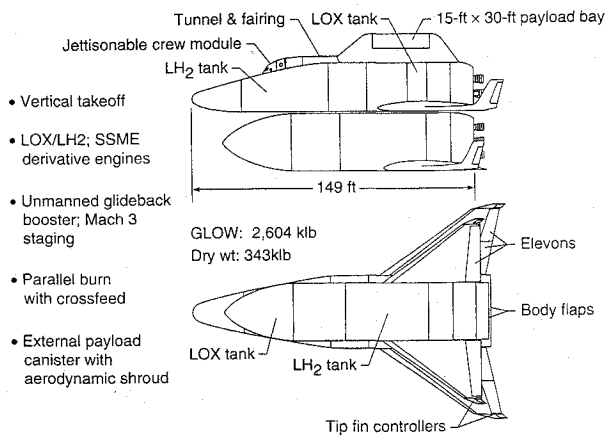

Fig. 3 AMLS two-stage vehicle configurations.

to be welded aluminum-lithium (Al/Li) 2095 structures that were machined from plate. External foam insulation is used on the surfaces requiring insulation, because internal cryogenic insulation was judged to be higher-risk. The cryogenic tanks and wing carry-through structure are separated as much as possible for simplicity in the tank construction. Because of the lack of experience in the use of reusable cryogenic tanks, the AMLS design philosophy maintains simple structural arrangements, stress patterns, and temperature distributions that may contribute to improved tank life.

Booster Description

The structural arrangement of the booster is shown in Fig. 4. The tank construction of the booster is similar to that of the external tank (ET) of the Space Shuttle system except for the use of the more advanced Al/Li 2095 material. The LO2 tank has a flat front bulkhead, an ogive forward section, a cylindrical body, and an ellipsoidal aft dome similar to the ET LO2 tank. The Al/Li 2095 intertank section is dry and contains the forward landing gear and support for the forward connection to the orbiter. The LH2 tank is cylindrical with fore and aft ellipsoidal domes. It requires more internal stiffening than the ET LH2 tank, because it is a primary compression (and bending) load path on the launch pad. The cryogenic tanks and intertank section are stiffened with internal Al/Li 2095 ring frames and stringers. The cylindrical section behind the LH2 tank is called the aft skirt. It is constructed of a short section of Al/Li 2095 to alleviate thermal distortion problems and a longer section of graphite polyimide (Gr/Pi) honeycomb that will withstand booster operating temperatures without insulation. It supports the thrust structure of the propulsion system and contains the primary wing attachments. The wing is also constructed of uninsulated Gr/Pi honeycomb with a nonstructural titanium leading edge. The primary landing-gear support is attached to the wing. The wing carry-through is attached to heavy frames in the aft skirt at the front and aft spars. The front of the wing root rib is attached to the fuselage by a vertical link. The Al/Li thrust structure is a conical shell in the upper portion with a flat shelf or beam supporting the three lower engines without attachment to the wing box or aft LH2 tank dome. There is a nonstructural Gr/Pi aerodynamic fairing between the wing and the fuselage.

Orbiter Description

The orbiter (shown in Fig. 5) differs structurally from the booster in that it employs dual-lobed main propellant tanks, a long, canted conical nose, and an aft-located LO2 tank. The nose of the orbiter is carbon-carbon supported by an insulated Gr/Pi shell. The forward landing gear is in the Gr/Pi honeycomb nose section. The LH2 tank is a welded Al/Li 2095 structure with Al/Li 2095 extensions on either end to provide thermal compatibility with Gr/Pi structure. The forward attachment between the orbiter and the booster is contained in the LH2 tank. The intertank structure is constructed of Gr/Pi honeycomb. The LO2 tank is constructed of Al/Li and carries some primary thrust loads. The Al/Li thrust structure in the orbiter is a truss structure design. Supports for the truss are attached to the longerons in the LO2 tank at the top and bottom of the web, which divides the two lobes, and to a heavy longeron that reacts the thrust

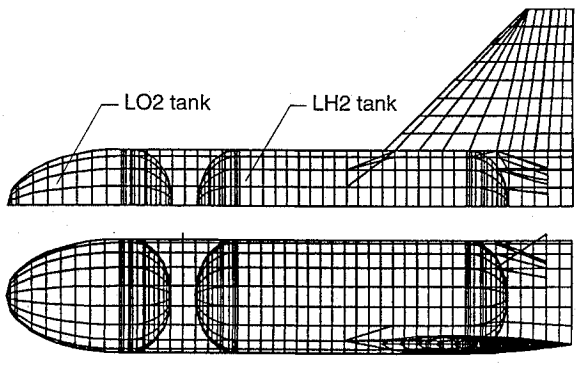

Fig. 4 Booster finite-element model.

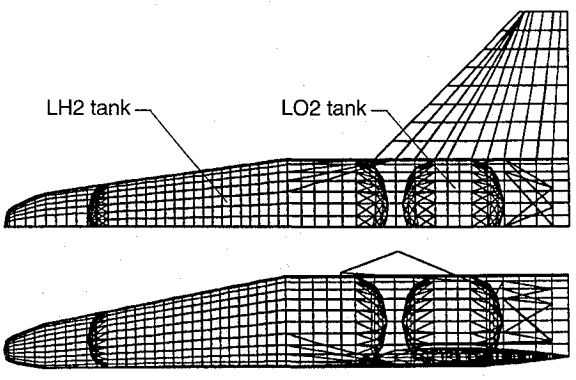

Fig. 5 Orbiter finite-element model.

loads transmitted from the booster and extends into the LO2-tank lower skin. The fuselage section behind the LO2 tank is again called the aft skirt. It is constructed of a short section of Al/Li 2095 to alleviate thermal distortion problems and a longer section of Gr/Pi honeycomb. It supports the thrust structure of the propulsion system and contains the primary wing attachments. The orbiter wing is also constructed of Gr/Pi honeycomb with a nonstructural advanced carbon-carbon leading edge. The primary landing-gear support is attached to the wing. The wing attachment is similar to that in the booster except that there is a forward beam through the intertank area. The orbiter also has nonstructural Gr/Pi aerodynamic fairings between the wing and fuselage and between the lobes of the LO2 and LH2 tanks. These fairings support the thermal protection system but must be attached to the tanks in a manner that will absorb the thermal shrinkage of the cryogenic tanks while maintaining the integrity of the thermal protection system. Since the payload container and crew cabin do not carry primary vehicle structural loads, they are modeled as masses that load the primary structure at a number of discrete points.

Results and Discussion

Trajectory Analysis

The nominal POST ascent trajectory for the vehicle is presented in Fig. 6. As shown in the figure, the initial T/W is about 1.3. As propellant is burned, the vehicle acceleration increases until it enters the transonic flight regime at high dynamic pressure (maximum of 700 psf) at about 60 s. The large increase in drag at this point causes the acceleration to decrease for a short period of time. The vehicle acceleration then increases until staging occurs at Mach 3 at an altitude of 71,000 ft. Vehicle trim and control during ascent are provided by gimbaling of the main engines of both vehicles. Because the booster is empty of propellant and the orbiter is fully loaded at staging, engine gimbal angles of up to 10 deg are required to trim the configuration. This leads to large thrust loads (up to 2.0 Mlb) being transferred between the vehicles. The unmanned booster then separates from the orbiter and performs an unpowered glide back to the launch site. These staging and glideback maneuvers are described in more detail in Ref. 9. The orbiter continues to accelerate until the longitudinal acceleration limit of 3 g is encountered at 300 s. The engines are throttled to maintain this limit until orbital insertion occurs at 420 s into a transfer orbit with a 50-n.mi. perigee

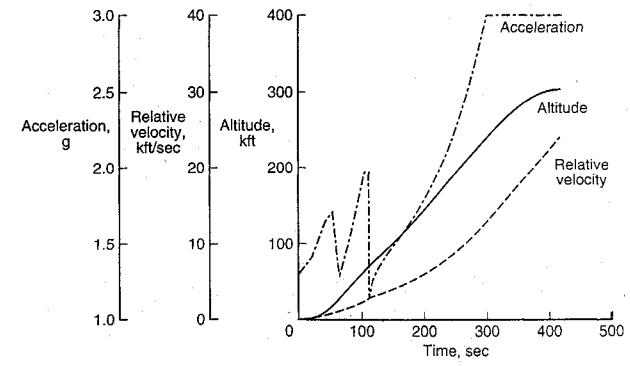

Fig. 6 AMLS ascent trajectory.

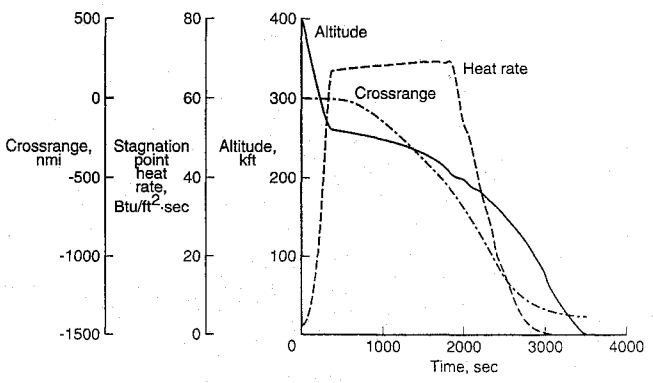

Fig. 7 AMLS entry trajectory.

and 100-n.mi. apogee. Further details on ascent trajectories for the AMLS vehicle are contained in Ref. 10.

The nominal POST entry trajectory for the fully reusable orbiter is presented in Fig. 7. After performing a deorbit burn, the vehicle reaches nominal atmospheric interface (altitude of 300,000 ft) at a relative flight-path angle of −1 deg and an angle of attack of 30 deg. Throughout the majority of the entry profile, the angle of attack of the orbiter remains between 25 and 30 deg to allow hypersonic trim, maximize lift-to-drag ratio, and minimize lee-side heating. POST was employed to determine a trajectory that minimized the maximum stagnation-point heat rate during entry while still achieving sufficient crossrange (1100 n.mi.) to allow for a once-around abort from a polar orbit. At an altitude of 260,000 ft, the equilibrium stagnation-point heat rate (based on a reference sphere with a 1-ft radius) reaches 65 Btu/ft^2·s. The bank angle of the vehicle is then modulated between 0 and 90 deg for about 1700 s to hold the heat rate below 69 Btu/ft^2·s. This was found to be the minimum value that the maximum stagnation-point heat rate could be limited to and still achieve the desired crossrange. When an altitude of 200,000 ft is reached, the bank angle gradually decreases, and the vehicle prepares for terminal energy-management maneuvers. Using this approach, the orbiter is capable of about 1300 n.mi. of crossrange. This entry analysis is used to size the nonstructural thermal protection system, which is sized to assure that the underlying vehicle structure remains within reasonable temperature ranges to insure adequate material strength.

Finite-Element Model Construction

The results from the APAS aerodynamic analysis (variation of vehicle lift coefficient, drag coefficient, and pitching-moment coefficient with Mach number and angle of attack) served as inputs to the POST trajectory analysis. The integrated loads on the vehicle due to thrust, gravity, and aerodynamic forces were then obtained from POST for a number of critical loading conditions. APAS was also used to help determine the distribution of the aerodynamic loads on the vehicles. The critical loading conditions selected include:

1) A lift-off condition with impact due to the sudden release of vehicle hold-down restraints.

2) A prelaunch condition without internal tank pressurization, to simulate on-the-pad conditions with ground winds.

3) A maximum-normal-force condition on the booster.

4) A condition just prior to staging when the maximum thrust is transmitted to the orbiter.

5) A Mach-3 separation maneuver on the orbiter.

6) A 2.5 g subsonic pullup maneuver.

7) A 2.0 g landing impact.

8) A material minimum-gauge condition.

The LO2-tank limit pressure utilized in the study was 22 psia, with an ultimate pressure of 33 psia. The LH2-tank limit pressure utilized in the study was 34 psia, with an ultimate pressure of 51 psia. In general, design ultimate loads of 1.5 times the applied loads were utilized. However, to increase vehicle reliability and provide longer life, it might be desirable to increase the operational load margins further. Increasing operational load margins could allow lifetime vehicle certification, similar to commercial airline practices, which would greatly reduce ground-operation manpower requirements.

Symmetric finite-element models of both the orbiter and booster vehicles were constructed for the study. The model of the booster (Fig. 4) has approximately 1250 joints and 1700 elements. The model of the orbiter (Fig. 5) has approximately 1600 joints and 2800 elements. The models were analyzed separately with constraints located at the attachment points on the orbiter. The connection between the vehicles is almost statically determinate, and reactions on the models were checked against inertial forces calculated from the POST trajectory program.

Each skin was modeled with a two-dimensional element having honeycomb sandwich properties, which is the most reliable two-dimensional element with membrane and bending stiffness in EZDESIT. The unstiffened skin in the tank domes was modeled with a very shallow core structure. Because all of the skin thickness in a sandwich is effective in both directions, the stiffened skin in the tank walls modeled with a core structure of sufficient depth to provide equivalent weight for the necessary longitudinal stiffeners in a T-shiffened skin.

Small frames were modeled with planar beam elements. Since the skin elements are large ($\approx$ 30 in. long), and skin curvature reduces the effective skin width actually contributing to the flange area, these elements were centered on the skin joints to prevent large amounts of skin area from contributing to the outer-flange stiffness of the frame. Large frames were modeled with quadrilateral elements for webs and with rods for interior flanges. Frames are located at every skin joint (row of nodes in the model) in the tank and consequently contribute to hoop strength as efficiently as the skin in the model. In an actual structure, the skin between frames would expand radially more than the frames. Additional core weight was included to compensate for this situation.

Tank pressure loads were modeled as distributed loads on the interior of the tanks. An approximation was made in the modeling of liquid-pressure-head loads by applying the loads for partially full conditions as pressures caused by a reduced-density liquid acting on the complete interior of the tank. This produces the correct maximum pressure but produces somewhat higher pressures in other areas.

Finite-Element Model Analysis

The booster and orbiter finite-element models were analyzed using EAL for the previously mentioned load cases. The models were then resized using the EZDESIT program to satisfy strength criteria. Four iterations of the analysis and resizing procedure were carried out to obtain a satisfactory strength design. The weights calculated by EZDESIT contain a user-specified nonoptimum factor or net-weight multiplier to approximate the weight of structural details not modeled in the finite-element model. The nonoptimum factor used in this study is 1.5, thus increasing the finite-element model weights by 50%. Linear bifurcation buckling analysis of both models showed that they buckled below design ultimate loads. The models were resized iteratively, using the procedure discussed in Appendix A, to increase the buckling strength to that it equaled or exceeded the design ultimate loads.

Booster Analysis

The strength-designed element weight per unit of area is shown in Fig. 8. Most of the vehicle surface skin weighs less than 2 psf.

Table 1 Booster-structure weight controlled by load case

Load case	% Weight
Liftoff with impact	58.4
Unpressurized tanks on pad	0.6
max $q\alpha$	15.5
Maximum thrust transfer	22.1
Subsonic pullup maneuver	2.8
Runway bump	0.6

Table 2 Booster-structure weight controlled by failure mode

Failure mode	% Weight
Minimum gauge	23.0
Panel buckling	9.2
Compressive yield	7.0
Yield	18.1
Ultimate	42.7
Overall buckling (additional)	+0.2

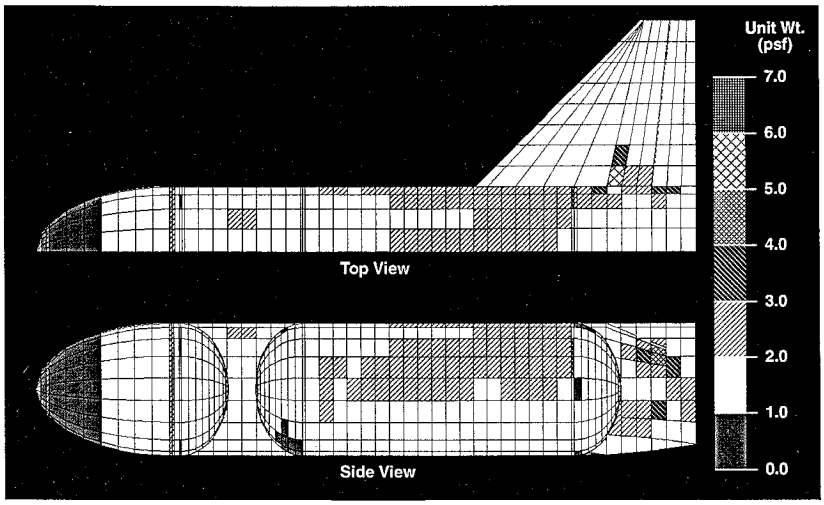

Fig. 8 Booster shell elements: weight per unit area.

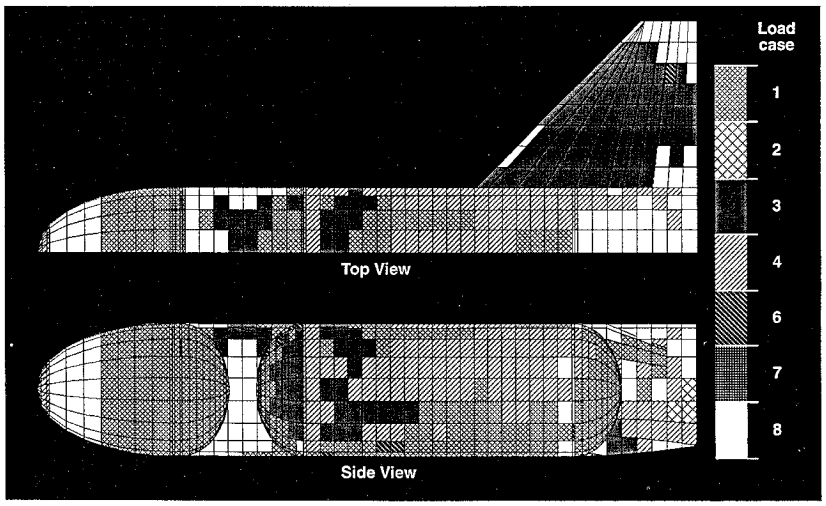

Fig. 9 Booster load cases: sizing shell elements.

However, frame and longeron weights are not included in these weights. A weight of 2 psf for the Al/Li structure is equivalent to an average skin thickness of 0.099 in. of Al/Li plus the 50% nonoptimum weight. In the LH2 tank, the ring frames add additional hoop material equivalent to an average skin thickness of 0.033 in. of material plus the 50% nonoptimum weight. The value of internal pressure multiplied by the radius of the LH2 tank is approximately 8000 lb/in.

Table 1 shows the percentage of booster structural weight for which a given loading condition produces the maximum load. The distribution of the strength-designed weights caused by the different load conditions are given in Fig. 9. The load-case members correspond to those described above in the "Finite-Element Model Construction" section. Load case 1, liftoff with the thrust impact due to instantaneous hold-down release, sizes elements that contribute to over half of the weight. This loading condition instantaneously removes a restraining force equal to 30% of the vehicle's weight. Alleviation of this impact load may be beneficial, but no estimate of the resulting weight savings has been made.

The sums of the strength-designed weights controlled by the different failure conditions are shown in Table 2. The small increment added to satisfy buckling constraints (not shown in Table 1) is also shown. The failure condition controlling the sizing of various elements is shown in Fig. 10. The minimum-gauge-sized structure, which constitutes about 20% of the total weight, is primarily in the lightly loaded portions of the wing, LO2 tank, intertank, and fairings. Overall a buckling does not appear to be significant in the booster.

The calculated weights for the components of the strength-designed booster model are shown in Appendix B. Also shown are the estimated component weights from the Space Shuttle ET, where applicable. The slosh baffle weight for the booster oxygen tank was obtained from the scaled ET. The LH2 and LO2 tanks are lighter than the scaled ET weights, as expected, because the Al/Li

Table 3 Orbiter-structure weight controlled by load case

Load case	% Weight
Liftoff with impact	6.8
Unpressurized tanks on pad	1.1
Maximum thrust transfer	14.1
Separation maneuver	16.5
Subsonic pullup maneuver	8.0
Runway bump	3.5

Table 4 Orbiter-structure weight controlled by failure mode

Failure mode	% Weight
Minimum gauge	39.2
Panel buckling	9.4
Compressive yield	12.4
Yield	14.2
Ultimate	24.8
Overall buckling (additional)	+4.8

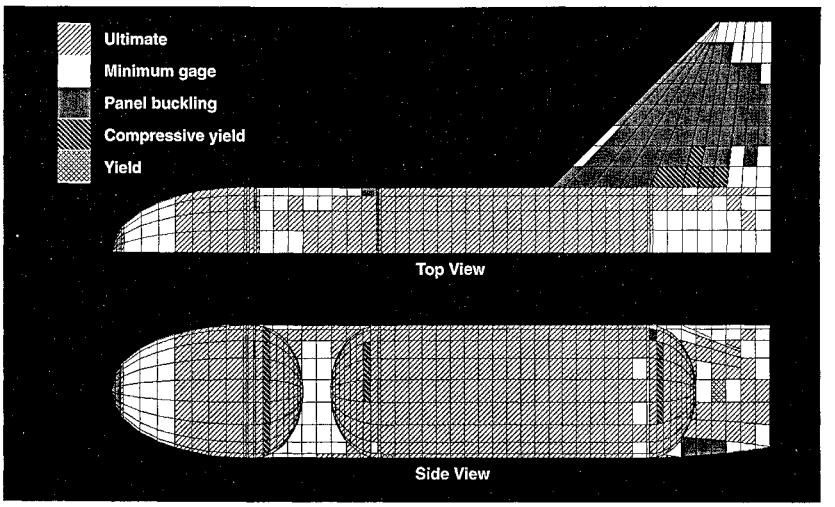

Fig. 10 Booster failure conditions controlling shell-element weights.

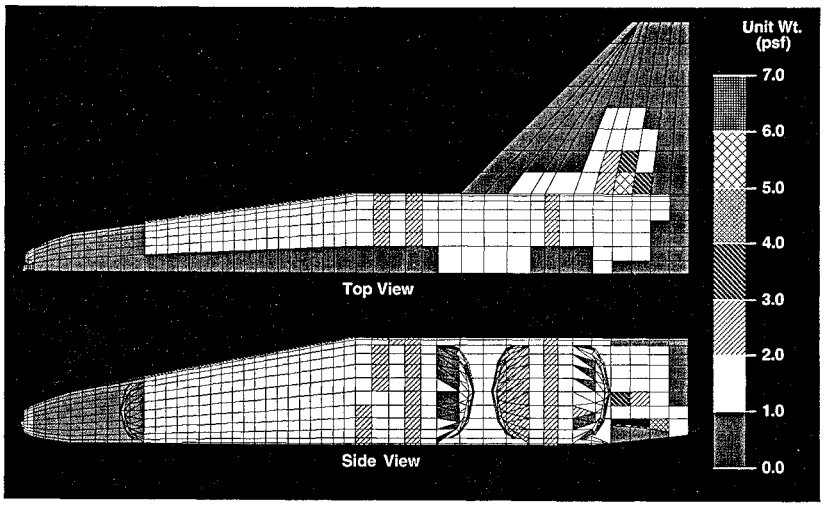

Fig. 11 Orbiter-shell elements: weight per unit area.

2095 alloy used on the booster is lighter, stronger, and stiffer than the 2219 alloy used in the ET. The intertank section is considerably lighter than the scaled ET value, because it is not subjected to the large thrust loads applied to the ET by the solid rocket boosters, nor does it have the transverse beam and large cutouts for the structure to support those loads.

Orbiter Analysis

The strength-designed weight per unit of area is shown in Fig. 11. Again, most of the vehicle surface skin weight is less than 2 psf. The webs between the two lobes of the tanks are not visible in the figure, but constitute a rather large portion of the tank weights.

Table 3 shows the percentage of booster structural weight for which a given loading condition produces the maximum load. The distributions of the strength-designed weights caused by the different load conditions are given in Fig. 12. The load-case numbers correspond to those described above in the "Finite-Element Model Construction" section. Load case 1, liftoff with the thrust impact due to instantaneous hold-down release, again sizes elements that contribute to over half of the weight.

The sums of the strength-designed weights controlled by the various failure conditions are shown in Table 4. The increment added to satisfy buckling constraints (not shown in Table 3) is shown as well. The failure condition controlling the sizing of various elements is shown in Fig. 13. The minimum-gauge-sized structure, which constitutes about 40% of the total weight, is primarily in the lightly loaded portions of the wing, the nose, the fairings, and the tank webs mentioned above. Overall buckling appears to be significant in the orbiter, causing a weight increase of 2800 lb. A large part of this weight increase is in the fairings over the valleys between the tank lobes. Remodeling these areas as fairings that only transmit applied pressure loads to the tanks would decrease the weight of the fairings but increase the axial load in the tanks. The effect of this change has not been investigated.

The calculated weights for components of the strength-designed orbiter model are shown in Appendix C. The unit weight of the or-

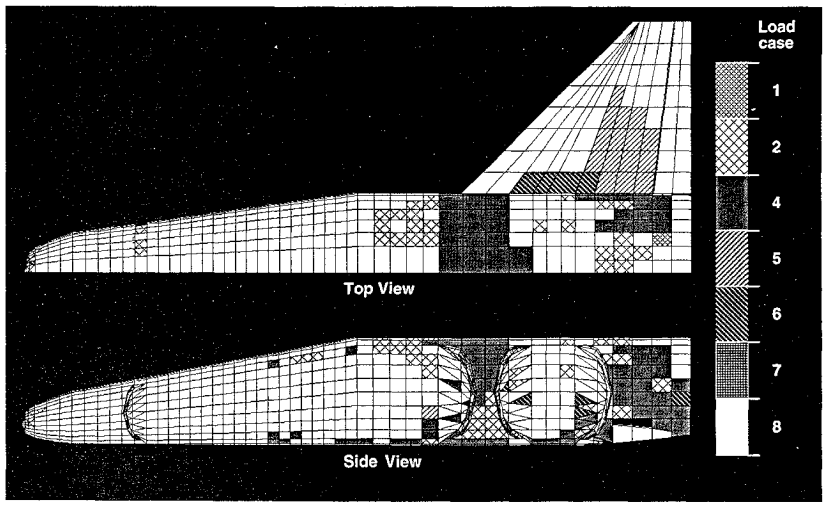

Fig. 12 Orbiter load cases: sizing shell elements.

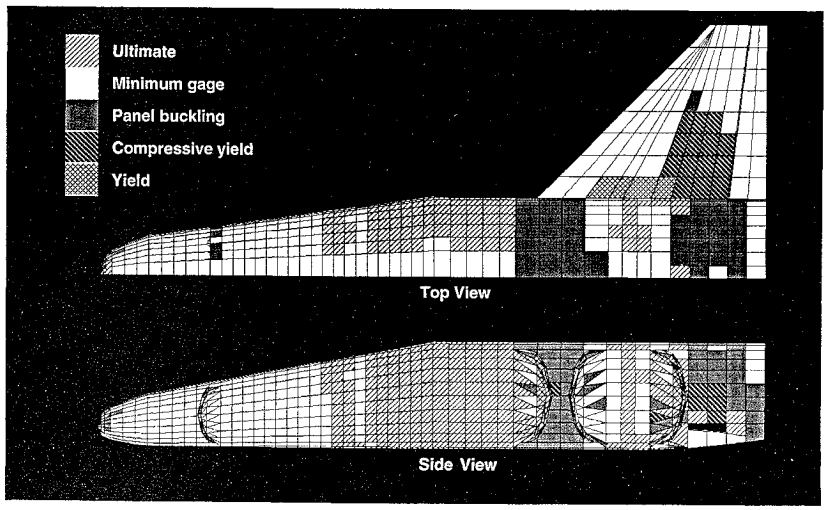

Fig. 13 Orbiter failure conditions controlling shell-element weights.

biter LO2 tank is similar to that of the booster. The unit weight of the orbiter LH2 tank is 3% heavier than that of the booster LH2 tank, despite the fact that it is lightly loaded relative to the booster LH2 tank, which must support the weight of the LO2 tank. The higher weight of the orbiter LH2 tank is largely due to the dual-lobe configuration that requires a center web structure between the lobes. The LH2 tank web is over 10% of the total tank weight. The intertank section is significantly lighter in unit weight ($\approx$ 50%) than the booster intertank, because it supports only the LH2 tank, which is about one-fifth the weight of the LO2 tank, and because it is constructed of Gr/Pi rather than Al/Li. The weight of the fairings over the valleys between the two lobes of the propellant tanks is approximately 1900 lb without consideration for buckling and is a disadvantage of employing a dual-lobe tank shape.

Conclusions

A structural analysis of a two-stage fully reusable AMLS vehicle has been made using near-term material technology. This preliminary analysis indicates that the structural concept is feasible. Because designs for a fully reusable launch vehicle can be very sensitive to weight growth, it is very important to perform detailed structural analyses as early as possible in the design cycle to evaluate the effect of evolutionary material technologies and to reduce program risk.

The loading condition that sizes most of the structural weight is the impact caused by the sudden release of vehicle hold-downs that removes, instantaneously, a restraining force equal to 30% of the vehicle's weight. Elimination or relaxation of vehicle hold-down requirements may be beneficial in reducing the vehicle structural weight, but would complicate vehicle control requirements at liftoff. The effect of reducing the impact load has not been determined for this concept.

The loads causing buckling of the strength-sized structures, determined from global bifurcation buckling analyses, were less than the applied loads. A resizing procedure was developed and applied to increase the buckling strength to a satisfactory level. Global buckling was found to be insignificant on the booster; however, resizing the structure to consider global bucking impacts on the orbiter increased the total structural weight by 5%.

A large portion of both the booster and the orbiter structure is lightly loaded. By weight, 20% of the booster structure and 40% of the orbiter structure use minimum-gage materials.

The dual-lobe main propellant tanks employed on the orbiter added significant structural weight that would not be required for cylindrical tanks. The central web in the orbiter liquid hydrogen tank is over 10% of the total tank weight. In addition, the weight of the fairings required between the two lobes of each tank is approximately 1900 lb, constituting over 3% of the vehicle structure.

An assumption was made that simple structural arrangements, primarily separation of tank pressure containment and wing bending restraint, would benefit cryogenic-tank life. Verification of this assumption and determination of other factors affecting cryogenic-tank life are necessary before building such a concept.

Appendix A: Buckling Resizing Method

The finite-element solution of the bifurcation buckling problem is expressed as

$$[K]\{\phi\} + \lambda[K_g]\{\phi\} = 0$$

where K is the global stiffness matrix, ϕ is the buckling mode shape (eigenvector), λ is the buckling eigenvalue, and K_g is the global geometric stiffness matrix. Although there are multiple eigenvalues and modes, usually it is desired to stiffen the structure so that the lowest buckling eigenvalue is greater than unity for the maximum applied load. If the equation is pre- and postmultiplied by a single mode shape,

$$\{\phi_1\}^T[K]\{\phi_1\} + 1\{\phi_1\}^T[K_g]\{\phi_1\} = 0$$

and if we use the usual normalization procedure where the term $\{\phi_1\}^T[K_g]\{\phi_1\}$ is -1.0, then the term $\{\phi_1\}^T[K]\{\phi_1\}$ becomes the eigenvalue. That term is also twice the strain energy (SE) caused by a displacement in that shape. This relationship may be used to develop a resizing algorithm by recognizing that in a simple column (a statically determinate structure with a fixed load distribution) the buckling load is directly proportional to the bending stiffness of the column.

The pre- and postmultiplied term $\{\phi_1\}^T[K]\{\phi_1\}$ is the summation of all the individual element stiffness terms (K_e), also pre- and postmultiplied:

$$\{\phi_1\}^T[K]\{\phi_1\} = \sum\{\phi_i\}^T[K_e]\{\phi_i\}$$

Hence, the elements having the largest strain energy for a given mode shape contribute the most to the corresponding eigenvalue. Because weight is the quantity to be minimized, it would appear that the elements having the largest strain energy per unit of weight will be most effective in increasing the buckling value for a given weight increase.

This procedure permits resizing of elements in the same way as fully stressed design does for strength sizing, but the sizing increment depends on the summation of element changes. The approach used is to normalize the elemental strain-energy densities for a mode shape, producing a data set N having values from 0.0 to 1.0, and assume a distribution for modification based on the normalized values. The distribution used herein assumes that each element will be incremented in dimension in proportion to its normalized strain-energy density. To prevent elements with small contributions from being incremented, the distribution may be truncated by neglecting elements below a minimum value.

An estimate of the eigenvalue change due to the application of the increments is

$$\Delta\lambda = 2\,\mathrm{SE}_{\max}\sum N_i^2$$

where $\mathrm{SE}_{\max}$ is the strain energy of the element having the largest strain-energy density. Because the estimated eigenvalue change is probably not the same as the difference between the desired value (DV) and the existing value, a scaling factor must be applied to the increments.

The magnitudes of the elemental changes are scaled using a factor equal to the required eigenvalue change divided by the change caused by the unscaled increment:

$$\text{Scale factor} = (\mathrm{DV} - \lambda_1)/\Delta\lambda$$

The required change is the difference between the desired value and the existing value. The desired value may be 1.0, or somewhat larger, because the resizing process causes the lower eigenvalues to become closely spaced and there may be a possibility of interaction. The magnitude of the maximum elemental change is limited by a preselected value (move limit), and other changes are scaled accordingly. Changes for several modes, caused by either a single loading with multiple eigenvalues less than 1.0 or several loadings with eigenvalues less than 1.0, may be made by summing the individual changes and imposing move limits on the summed changes.

Appendix B: Booster Strength-Sized Weights

Component	Study weight, lb	Scaled ET weight, lb
LO2 tank	6,751	8,336
Shell structure	3,027	4,645
Aft ring	732	503
Aft dome	1,435	1,631
Slosh baffles	1,557	1,557
Intertank	4,667	6,506
Skin	3,436	4,194
Attachment flange	0	380
Frames	1,089	931
Connection structure	142	646
Miscellaneous	0	355
LH2 tank	15,919	18,003
Forward dome	979	1,161
Barrel skin	8,801	11,675
Barrel frames	5,073	3,446
Aft dome	1,066	1,721
Wing	8,846	
Upper skin	2,409	
Lower skin	2,209	
Ribs and spars	2,170	
Center section	2,058	
Aft fuselage	12,199	
Skin	4,319	
Frames	2,672	
Thrust structure	3,474	
Wing fairing	1,734	
Booster orbiter connection	1,445	
Total structure	49,827	

Appendix C: Orbiter Strength-Sized Weights

Component	Study weight, lb
LH2 tank	19,595
Forward dome	400
Barrel skin	11,504
Barrel frames	6,100
Aft dome	1,591
Intertank	3,063
Skin	2696
Frames	367
LO2 tank	8,127
Forward dome	1,025
Barrel skin	2,950
Barrel frames	1,058
Aft dome	1,537
Slosh baffles	1,557
Fairings	4,494
LH2 tank	1,405
LO2 tank	488
Wing	2,601
Nose section	1,657
Nose cap	104
Front gear attachment	13
Skin	1,321
Frames	219
Wing	13,424
Upper skin	3,041
Lower skin	3,035
Ribs and spars	2,711
Center section	4,637
Aft fuselage	7,024
Skin	3,273
Frames	968
Thrust structure	2,783
Total structure	57,384

The advantages of the method are that it is relatively simple, does not require additional optimization programs, considers individual elements, and requires only the extraction and scaling of the strain-energy densities after the buckling calculations. Furthermore, the distribution of strain-energy density between axial and bending components may be used to assist in element sizing. At the expense of a larger number of elements, individual play orientations may be evaluated in a composite structure. The disadvantages of the method are that the analyst must decide how to apply it and interact with the solution process to determine when convergence has occurred. Also, because the process is sequential in nature, there is no guarantee of obtaining an optimum solution.

References

[1]Stone, H. W., and Piland, W. M., "An Advanced Manned Launch System Concept," International Astronautical Federation Paper 92-0870, Sept. 1992.

[2]Freemen, D. C., Talay, T.A., Stanley, D. O., and Wilhite, A. W., "Design Options for Advanced Manned Launch Systems," AIAA Paper 90-3816, Sept. 1990.

[3]McMillin, M. L., Rehder, J. J., Wilhite, A. W., Schwing, J. L., Spangler, J., and Mills, J. C., "A Solid Modeler for Aerospace Vehicle Preliminary Design," AIAA Paper 87-2901, Sept. 1987.

[4]Brauer, G. L., Cornick, D. E., and Stevenson, R., "Capabilities and Applications of the Program to Optimize Simulated Trajectories," NASA CR-2770, Feb. 1977.

[5]Divan, P. E., "Aerodynamic Analysis System for Conceptual and Preliminary Analysis from Subsonic to Hypersonic Speeds," AIAA Paper 80-1897, Aug. 1980.

[6]Anon., "PATRAN Plus User's Manual," Release 2.3, PDA Engineering, Pub. 2191020, Costa Mesa, CA, July 1988.

[7]Whetstone, W. D., "Engineering Analysis Language Reference Manual," EISI, San Jose, CA, July 1983.

[8]Cerro, J. A., and Shore, C. P., "EZDESIT, A Computer Program for Structural Element Sizing and Vehicle Weight Prediction," National Aero-Space Plane CR-1092, July 1990.

[9]Naftel, J. C., and Powell, R. W., "Aerodynamic Separation and Glideback of a Mach 3 Staged Booster," AIAA Paper 90-0223, Jan. 1990.

[10]Stanley, D. O., Talay, T. A., Lepsch, R. A., Morris, W. D., and Wurster, K. E., "Conceptual Design of a Fully Reusable Manned Launch System," *Journal of Spacecraft and Rockets*, Vol. 29, No. 4, 1992, pp. 529–537.